Building and Environment 85 (2015) 61–72

Contents lists available at ScienceDirect

Building and Environment

journal homepage: www.elsevier.com/locate/buildenv

Numerical investigation on particle deposition enhancement in duct air flow by ribbed wall

Hao Lu, Lin Lu*

Department of Building Services Engineering, The Hong Kong Polytechnic University, Hung Hom, Kowloon, Hong Kong, China

ARTICLE INFO

Article history:
Received 9 October 2014
Received in revised form
11 November 2014
Accepted 24 November 2014
Available online 4 December 2014

Keywords:
Particle deposition
Surface ribs
Deposition enhancement
RSM model
CFD

ABSTRACT

This paper studied the particle deposition in turbulent duct air flows with smooth and ribbed walls numerically. The RSM model with turbulent fluctuation correction and Lagrangian track method were adopted to investigate the particle deposition enhancement by ribbed surface. The air flow velocity profiles for both smooth and ribbed-ducts as well as particle deposition velocity on smooth wall obtained in the present simulation were validated by agreeing well with the previous related study data. Particle deposition is significantly enhanced by surface ribs, especially in turbulent diffusion and eddy diffusion-impaction regimes. It is found that the captures of turbulent eddies induced by ribs and entrainments of large turbulent kinetic energy (T.K.E.) to the wall are the main mechanism for deposition enhancement of small particles. Moreover, pressure drop-weighted efficiency ratio of particle deposition enhancement for ribbed surface is evaluated in this study. The efficiency ratio for ribbed surface can reach more than 100 for particle sizes 0.2–3 μm but only about 2–3 for particle sizes 20–50 μm. This study shows that the repeated ribs on the surface could be an effective and efficient choice for particle deposition enhancement, especially for micron-meter particles.

1. Introduction

Air pollution has been becoming a serious problem in urban environment nowadays. Since people spend most of their time indoors, the particulate matter (PM) in the indoor environment can be a major threat to people's health. Therefore, effective and efficient particle removal devices become extremely necessary to improve indoor air quality (IAQ). It has been found that the repeated surface ribs can significantly increase the collection performance of the particle removal devices such as air electrostatic precipitators (ESP) [1,2]. This is because arrangement of repeated ribs on the ESP surface can intercept a large number of airborne particles. However, the extra pressure drop is also induced by the surface ribs for their form drag. Therefore, the comprehensive performance needs to be investigated and evaluated by considering the above effects. Moreover, Lai et al. [3,4] proposed that it may be an effective alternative to filtration through enhancing aerosol particle deposition by repeated surface ribs along the length of the ventilation duct. In fact, it had been found that plenty aerosol particles would be deposited in the ventilated bend according to the previous experimental studies by Sun and Lu [5,6]. If a large number of aerosol particles can be collected and deposited in a length of dismountable ventilation duct, the IAQ would be significantly improved which is favorable for people's health. Nevertheless, it is also conceivable that the pressure drop would be increased by the surface ribs, which should be considered for the comprehensive performance of particle deposition enhancement. Therefore, better understanding of particle deposition enhancement performance and mechanism in obstructed air flow is meaningful and valuable for IAQ and relative engineering designs and applications.

The previous studies of particle deposition enhancement performance by ribbed surface are limited. Lai et al. [3,4] studied the particle deposition enhancement in duct air flow by surface ribs experimentally. Their results indicated that particle deposition rate could be significantly enhanced by ribbed wall. Li et al. [7] numerically investigated the aerosol particle transport and deposition in a duct with an obstructing block. They found that large numbers of particles deposited on the blocks due to impaction and interception. Iacono et al. [8] predicted spherical and cylindrical particle motions in channel flow with one surface rib using large eddy simulation (LES). They found that spherical particles tend to

* Corresponding author. Tel.: +852 34003596.
E-mail address: vivien.lu@polyu.edu.hk (L. Lu).

http://dx.doi.org/10.1016/j.buildenv.2014.11.031
0360-1323/

accumulate on the windward rib surface while cylindrical particles don't. Hussein et al. [9] proposed a new particle deposition model for rough surface based on the three-layer deposition model [10–13]. Their results showed that the new model was capable to predict the deposition velocities on various rough surfaces. Recently, multilayer particle deposition in ribbed channel flow was investigated experimentally by Barth et al. [14] and numerically by Lecrivain et al. [15], however, the particle deposition enhancement was not investigated. In summary, it has been previously found that particle deposition velocity could be enhanced by ribbed surface. However, the studied particle sizes in the previous studies were mainly ranging from 0.7 to 7.1 μm. The other size particles from the turbulent diffusion regime to the inertia-moderated regime have been not examined. Furthermore, the interception of the ribs and the increase of deposition surface area have been found as the main mechanisms of such kind of enhancement [3,4,7]. However, the mechanisms from the view of the modification of flow structures and turbulent kinetic energy (T.K.E.) by ribbed surface are not well investigated. Therefore, particle deposition enhancement performance and mechanism by ribbed surface were not fully understood. Further investigation on the enhancement is recommended.

In general, experiment investigation and numerical simulation are the two main methods to investigate particle deposition on the wall. According to the review by Chen [16], numerical simulation method has been contributed about 70% of literature for the studies of ventilation performance prediction for buildings in 2007. This is because numerical simulation can predict the information of airflow, particle deposition and behavior in details [17,18]. Nevertheless, it is quite challenging to accurately measure and analyze particle deposition and movement in the near-wall region by experiments as many complex influencing factors are coupled together to affect particle behavior in practice. For numerical simulation, the Eulerian–Lagrangian methods have been considered as a powerful tool to investigate the particle deposition in turbulent flow by a number of studies such as Tian and Ahmadi [19], Zhang and Chen [20], Gao et al. [21], Jiang et al. [22–24], and Sun et al. [25–27]. In these methods, turbulent flow is treated as a continuous phase and simulated in the Eulerian frame while particles are considered as a discrete phase and the trajectory of each particle is tracked through solving the particle dynamic equation. It has been found that accurate prediction of turbulent air flow is very important for successfully simulating the particle deposition onto surface [19,20]. Tian and Ahmadi [19] numerically studied the particle deposition in duct flow by using different turbulence models. It was found that Reynolds stress model (RSM) with the correction of turbulent wall-normal velocity fluctuation can simulate the particle deposition velocity in turbulent channel flow more accurately compared with the other RANS models. This is because most eddy viscosity turbulence models such as k-ε and k-ω assume isotropic turbulence structures while RSM considers anisotropy of turbulence. Therefore, the RSM can predict the turbulent flow more accurately with strong anisotropy behaviors such as the flow over ribbed surface. Moreover, although direct numerical simulation (DNS) or large eddy simulation (LES) can obtain more accurate turbulent flow fields, it also needs much more computational costs compared with RANS. As RSM with velocity fluctuation correction can already accurately predict deposition velocity of particles with 0.1–50 μm in turbulent flow [19], it is unnecessary to use DNS or LES for large calculation amount. Therefore, RSM with turbulent fluctuation correction is employed to perform the simulations.

In the present study, particle depositions on both smooth and ribbed surfaces are investigated by RSM turbulence model with turbulent fluctuation correction and Lagrangian tracking method. This study aims to investigate the enhancement ratio and mechanism of particle deposition by ribbed surface with comparison with smooth surface case. Moreover, pressure drop-weighted particle collection efficiency by ribbed wall is defined and evaluated to provide guides for the relative engineering designs and applications. The particle sizes in this study are ranging from 0.1 to 50 μm including the turbulent diffusion regime to the inertia-moderated regime.

2. Numerical model and methodology

In the present study, the commercial software Ansys Fluent 13.0 implemented with user-defined functions (UDF) was employed for the simulation since its capacity and reliability have been widely proved in many studies [19–27].

2.1. Turbulent air flow model

The RSM model was adopted to deal with turbulent air flow because it accounts for the anisotropy of turbulence. The mean continuity and momentum equations are given to describe incompressible turbulent flow as follows.

$$\frac{\partial \overline{u}_i}{\partial x_i} = 0, \tag{1}$$

$$\frac{\partial \overline{u}_i}{\partial t} + \overline{u}_j \frac{\partial \overline{u}_i}{\partial x_j} = -\frac{1}{\rho}\frac{\partial \overline{p}}{\partial x_i} + \frac{1}{\rho}\frac{\partial}{\partial x_j}\left(\mu \frac{\partial \overline{u}_i}{\partial x_j} - \rho \overline{u_i' u_j'}\right), \tag{2}$$

where $\overline{u}_i$ is the time-averaged velocity, $\overline{p}$ is the time-averaged pressure, μ is the dynamic viscosity of air, and $\rho\overline{u_i'u_j'}$ is the Reynolds stress tensor. The transport equation of the Reynolds stress is given as follows,

$$\frac{\partial}{\partial t}\left(\overline{u_i'u_j'}\right) + \overline{u}_k \frac{\partial}{\partial x_k}\left(\overline{u_i'u_j'}\right) = \underbrace{\frac{\partial}{\partial x_k}\left(\frac{\nu_t}{\sigma_k}\frac{\partial \overline{u_i'u_j'}}{\partial x_k}\right)}_{D_{T,ij}=\text{Turbulent Diffusion}} \underbrace{-\left(\overline{u_i'u_k'}\frac{\partial \overline{u}_j}{\partial x_k} + \overline{u_j'u_k'}\frac{\partial \overline{u}_i}{\partial x_k}\right)}_{P_{ij}=\text{Stress Production}} \underbrace{-C_1\frac{\varepsilon}{k}\left[\overline{u_i'u_j'} - \frac{2}{3}\delta_{ij}k\right] - C_2\left[P_{ij} - \frac{2}{3}\delta_{ij}P\right]}_{\phi_{ij}=\text{Pressure Strain}} - \underbrace{\frac{2}{3}\delta_{ij}\varepsilon}_{\varepsilon_{ij}=\text{Dissipation}} \tag{3}$$

where the production term is given as

$$P_{ij} = -\left(\overline{u_i'u_k'}\frac{\partial \overline{u}_j}{\partial x_k} + \overline{u_j'u_k'}\frac{\partial \overline{u}_i}{\partial x_k}\right), \quad P = \frac{1}{2}P_{ii}, \quad \delta_{ij} = \begin{cases} 1 & (i=j) \\ 0 & (i \neq j) \end{cases} \tag{4}$$

In the Eq. (3), empirical constants $\sigma_k = 1.0, C_1 = 1.8$ and $C_2 = 0.6$ [28]. Moreover, the turbulence dissipation rate ε is calculated by the following transport equation,

$$\frac{\partial \varepsilon}{\partial t}+\overline{u}_j\frac{\partial \varepsilon}{\partial x_j}=\frac{\partial}{\partial x_j}\left[\left(\nu+\frac{\nu_t}{\sigma_\varepsilon}\right)\frac{\partial \varepsilon}{\partial x_j}\right]-C_{\varepsilon 1}\frac{\varepsilon}{k}\overline{u_i'u_j'}\frac{\partial \overline{u}_i}{\partial x_j}-C_{\varepsilon 2}\frac{\varepsilon^2}{k} \quad (5)$$

where empirical constants in the Eq. (5) $\sigma_\varepsilon = 1.3, C_{\varepsilon 1} = 1.44$ and $C_{\varepsilon 2} = 1.92$.

It has been found that near-wall modeling for turbulent flow is crucial for simulating particle deposition accurately [19]. In the present study, the two-layer zonal model combined with enhanced wall function were employed to deal with the flow in near-wall region because this method could possess the accuracy of the standard two-layer approach for fine near-wall meshes [25]. In the viscosity-affected near-wall region, the Wolfstein's one-equation model [29] was employed. The turbulent viscosity is computed as follows,

$$\mu_{t,2\text{layer}} = \rho C_\mu l_\mu \sqrt{k} \quad (6)$$

Besides, the dissipation rate ε is calculated by

$$\varepsilon = \frac{k^{3/2}}{l_\varepsilon} \quad (7)$$

where the length scales l_μ and l_ε in the Eqs. (6) and (7) are calculated referring to Chen and Patel [30], The turbulent viscosity in Eq. (6) is blended with the high Reynolds number μ_t defined in the outer region, as proposed by Jongen [31],

$$\mu_{t,\text{enh}} = \lambda_\varepsilon \mu_t + (1-\lambda_\varepsilon)\mu_{t,2\text{layer}} \quad (8)$$

where λ_ε is the blending function. More details of the two-layer zonal model combined with enhanced wall functions can be found in Ansys Fluent 13 [32].

2.2. Particle motion model

Lagrangian trajectory method tracks individual particle motion by solving the particle momentum equation. In this study, the particulate flow was assumed to be dilute enough so that the modification of particles on turbulent air flow and the interactions between particles are ignored. The equation of particle motion is as follows,

$$\frac{du_p}{dt} = \frac{1}{\tau}\frac{C_D \mathrm{Re}_p}{24}(u_g - u_p) + \frac{g(\rho_p - \rho_g)}{\rho_p} + F_B + F_S \quad (9)$$

Here, u_g and u_p are the velocity of fluid and particle, respectively. ρ_g is the density of fluid and ρ_p is the density of particle. On the right-hand side of Eq. (9), the drag force, the gravity, the buoyancy force, the Brownian force F_B and the Saffman's lift force F_S are accounted. The Brownian force F_B is given by,

$$F_B = \zeta\sqrt{\frac{\pi S_0}{\Delta t}} \quad (10)$$

where $S_0 = 216\rho\nu k_b T/\pi\rho_p^2 d_p^5 C_C$. The Saffman's lift force F_S is given as follows,

$$F_S = \frac{2\rho K_c \nu^{0.5}}{\rho_p d_p (S_{lk}S_{kl})^{0.5}} s_{ij}(u - u_p) \quad (11)$$

The relaxation time of particle in Eq. (9) is calculated by,

$$\tau = \frac{S d_p^2 C_C}{18\nu} \quad (12)$$

S is the ratio of particle-to-fluid density. C_C is the Cunningham slip correction factor, which is calculated by Ref. [33],

$$C_C = 1 + \frac{2\lambda}{d_p}\left(1.257 + 0.4e^{-(1.1d_p/2\lambda)}\right) \quad (13)$$

The drag coefficient C_D is given as,

$$C_D = \frac{24}{\mathrm{Re}_p}, \quad \text{for} \quad \mathrm{Re}_p < 1 \quad (14)$$

and

$$C_D = \frac{24}{\mathrm{Re}_p}\left(1 + 0.15\mathrm{Re}_p^{0.687}\right), \quad \text{for} \quad 1 < \mathrm{Re}_p < 400 \quad (15)$$

2.3. Turbulent dispersion of particles

Turbulent dispersion of particle, which is caused by turbulent instantaneous fluctuation, is an important mechanism for particle dispersion and deposition. In this study, Discrete Random Walk Model (DRW) was adopted to simulate particle turbulent dispersion. DRW model allows successive encounter of particles with turbulent eddies by a Gaussian distributed random velocity fluctuation of fluids and a time scale of turbulent eddy [32]. The turbulent fluctuating velocity is given as,

$$u' = \zeta u'_{\text{rms}}, \; v' = \zeta v'_{\text{rms}}, \; w' = \zeta w'_{\text{rms}} \quad (16)$$

where ζ is normal distributed random number with zero mean and unit variance; and u'_{rms}, v'_{rms} and w'_{rms} are fluctuating velocities obtained by the RSM model respectively. The time scale of a turbulent eddy is given as below,

$$\tau_e = 2T_L \quad (17)$$

where the fluid Lagrangian integral time scale is calculated by,

$$T_L \approx 0.3\frac{k}{\varepsilon} \quad (18)$$

Previous studies have shown that the wall-normal turbulent fluctuating velocity is crucial for the accurate simulation of particle deposition velocity [19,20]. For particle deposition on smooth surface, Tian and Ahmadi [19] adopted a correction of wall-normal fluctuation v'_{rms} in the near-wall region from the DNS data by Kim et al. [34]:

$$\frac{v'_{\text{rms}}}{u^*} = C\left(y^+\right)^2, \quad \text{for} \quad y^+ < 4 \quad (19)$$

where u^* is frictional velocity, and the value of the constant C is suggested to be 0.008. y^+ in the Eq. (19) is dimensionless distance from the wall, which can be defined as follows,

$$y^+ = \frac{yu^*}{\nu} \quad (20)$$

For particle deposition on ribbed surface, the correction Eq. (21) was employed in the study as it had been successfully applied for multilayer deposition simulation on ribbed channel flow by Lecrivain et al. [15], as below:

$$\frac{v'_{\text{rms}}}{u^*} = \frac{a_1 y^{+2}}{1 + b_1 y^+ + c_1 y^{+2.41}}, \quad \text{for} \quad y^+ < 30 \quad (21)$$

In the Eq. (23), $a_1 = 0.0116$, $b_1 = 0.203$ and $c_1 = 0.0014$.

2.4. Particle deposition velocity

The particle deposition velocity was adopted to evaluate the particle deposition process, given as:

$$V_d = \frac{J}{C_0} \tag{22}$$

where J is defined as the number of particles deposited per unit time and unit area of the surface, and C_0 represents the mean particle concentration. In the numerical simulation, the particle deposition velocity V_d can be estimated by,

$$V_d = \frac{N_d/t_d/A}{N_0/V} = \frac{N_d/t_{\max}}{N_0/h} \tag{23}$$

The relationship between the non-dimensional particle deposition velocity and dimensionless particle relaxation time has been commonly employed to evaluate the efficiency of particle deposition [35]. The dimensionless particle deposition velocity can be calculated as,

$$V_d^+ = \frac{V_d}{u^*} \tag{24}$$

where frictional velocity u^* can be calculated by,

$$u^* = \sqrt{\tau_w/\rho_g} = U_{\text{mean}}\sqrt{f/2} \tag{25}$$

The dimensionless particle relaxation time can be calculated by,

$$\tau_p^+ = \frac{C_C S d_p^2 u^{*2}}{18\nu^2} \tag{26}$$

3. Case description

For particle deposition on smooth wall, the two-dimensional (2D) computational duct is shown in Fig. 1(a) with 0.02 m high and 0.4 m long. The calculation domain and the flow conditions were in accordance with those designed by Tian and Ahmadi [19] as well as Zhang and Chen [20] in order to further compare with their simulation results. Structured grids, shown in Fig. 1(b), were used to discretize the computational domain with 400 × 80 cells in streamwise and wall-normal directions, respectively. The first grids are 0.05 mm away from the wall and y^+ for the first grids is about 1.13 in wall units. The grid spacing evolves to the center region with a growth factor of 1.2 in wall-normal direction. An enlarged view of the grids near the wall is shown in Fig. 1(c).

For particle deposition on ribbed wall, the computational duct is shown in Fig. 2(a). The duct size is the same with the smooth duct

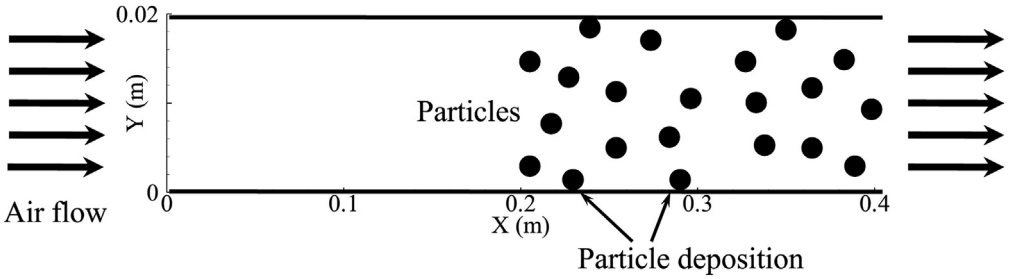

(a) Schematic view of the gas-particle flow in smooth-wall duct

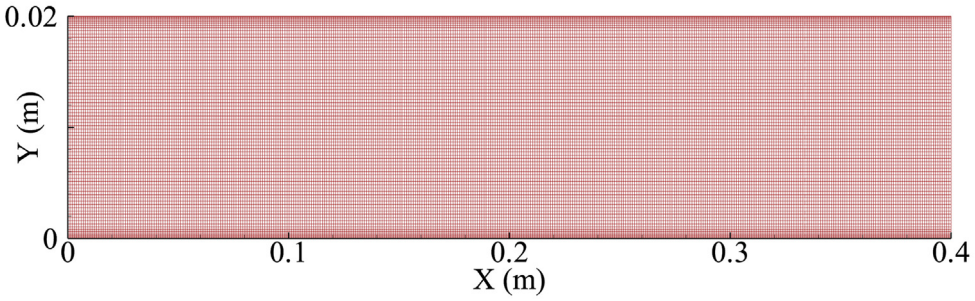

(b) Computational grids for duct with smooth wall

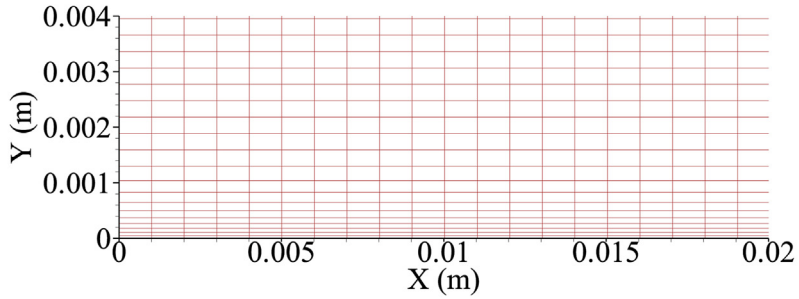

(c) A closer view of the grids near the lower wall.

Fig. 1. Geometrical and grid information of the duct with smooth wall.

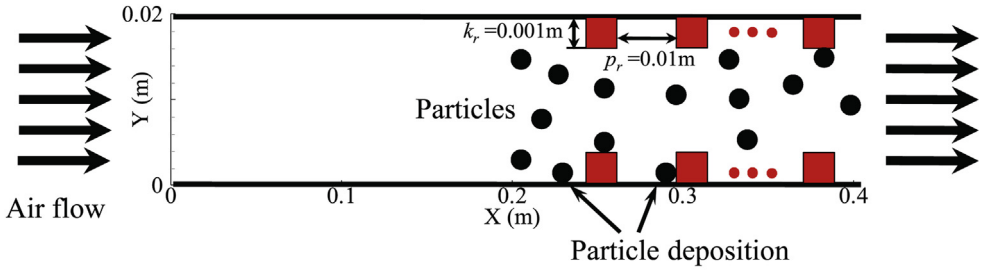

(a) Schematic view of the gas-particle flow in ribbed-wall duct

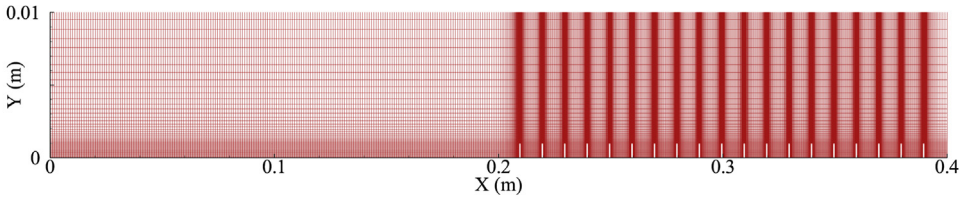

(b) Computational grids for duct with ribbed wall

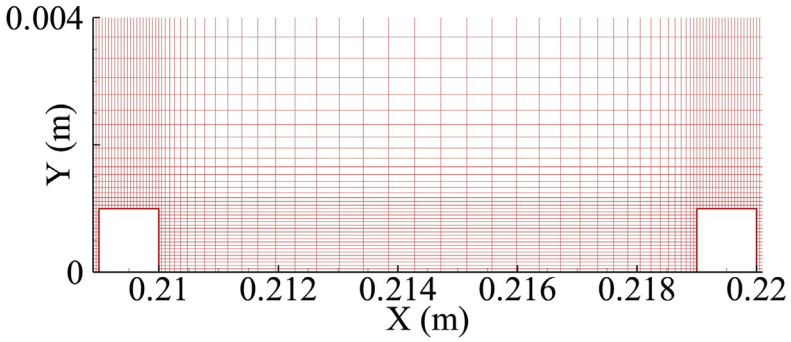

(c) A closer view of the grids between two adjacent ribs

Fig. 2. Geometrical and grid information of the duct with ribbed wall.

for comparison. The first half of the channel is smooth to ensure full development of turbulent air flow, while 19 ribs were arranged on the last half of the channel walls with identical spacing in streamwise direction. Half of computational domain was simulated to reduce calculation cost as the ribbed-duct is symmetrical. A total number of 110,000 structured grids were employed for the simulation of ribbed-duct flow, as shown in Fig. 2(b). The grids are clustered near the ribs and walls to accurately solve the complex turbulent flow in boundary layer. The first grids away from the walls and ribs are 0.05 mm. A closer view of the grids between two adjacent ribs can be seen in Fig. 2(c). Liou et al. [36] and Okamoto et al. [37] have found that the maximum enhancement of heat transfer with lowest pressure increase occurs when the spacing to height ratio p_r/k_r is around 10. This p_r/k_r ratio was also adopted in the experimental study of particle deposition enhancement by Lai et al. [3,4]. In this study, the ratio of the rib spacing to height p_r/k_r was also chosen as 10. Moreover, the rib-to-duct height ratio is usually from 0.02 to 0.1 in heat transfer enhancement by surface ribs [36]. The rib height k_r in this study is selected as 1 mm, which is 1/10 of the half height of the duct. This is consistent with the experiment case by Casara [38] for verifying the simulation results of turbulent air velocities. The boundary layer thickness is normally defined as the distance from the solid wall at which the viscous flow velocity is 99% of the freestream velocity [39,40]. In smooth duct, the turbulent boundary layer would be developed downstream from the inlet and the boundary layer thickness would become thicker along the streamwise direction. An empirical formula of the turbulent boundary layer thickness for smooth flat plate can be estimated as follows [39,40]:

$$\delta_{99} = 0.376X\frac{1}{\sqrt[5]{\mathrm{Re}_X}} = \frac{0.376\mu^{1/5}X^{4/5}}{\rho^{1/5}u_\infty^{1/5}} \tag{27}$$

where the X in the Eq. (27) is the streamwise distance from the inlet of the duct. According to the above equation, the boundary layer thickness at $X = 0.2$ m of the duct can be calculated as about 8 mm. Therefore, the surface rib height is much smaller than the local boundary layer thickness. It indicates that the ribs are completely covered in the turbulent boundary layer. The rib spacing p_r is 10 mm.

A total number of 48 cases were calculated, as shown in Table 1. In the present study, The dynamic viscosity of air μ is 1.789×10^{-5} kg s/m and the density of air is 1.225 kg/m^3 at $T = 288$ K. The air velocity is 5.5 m/s. Therefore, the Reynolds number based on the mean flow velocity and channel height is 7534.

To impose a fully developed velocity and T.K.E. profiles, user-defined boundary conditions were adopted in duct inlet [19]. The one seventh power law was employed as follows,

Table 1
Computational cases.

Case No.	Air velocity (m/s)	Particle diameter (μm)	Surface type	Position
1–12	5.5 m/s	0.1,0.2,0.3,0.5,1,2,3,5,10,20,30,50	Smooth	Vertical
13–24	5.5 m/s	0.1,0.2,0.3,0.5,1,2,3,5,10,20,30,50	Ribbed	Vertical
25–36	5.5 m/s	0.1,0.2,0.3,0.5,1,2,3,5,10,20,30,50	Smooth	Horizontal
37–48	5.5 m/s	0.1,0.2,0.3,0.5,1,2,3,5,10,20,30,50	Ribbed	Horizontal

$$U = U_{\text{free}}\left(\frac{y}{h/2}\right)^{1/7} \quad \text{for} \quad y \le h/2 \tag{28}$$

$$U = U_{\text{free}}\left(\frac{h-y}{h/2}\right)^{1/7} \quad \text{for} \quad y > h/2 \tag{29}$$

$$U_{\text{free}} = \frac{8}{7}U_{\text{mean}} \tag{30}$$

where U_{mean} is the mean velocity of the duct air flow and h is the duct height. The T.K.E. k [19]is given by,

$$k = \frac{\tau_w}{\rho_g\sqrt{C_\mu}} + \frac{y}{h/2}\left(0.002U_{\text{free}}^2 - \frac{\tau_w}{\rho_g\sqrt{C_\mu}}\right) \text{ for } 0 \le y \le h/2 \tag{31}$$

$$k = \frac{\tau_w}{\rho_g\sqrt{C_\mu}} + \frac{h-y}{h/2}\left(0.002U_{\text{free}}^2 - \frac{\tau_w}{\rho_g\sqrt{C_\mu}}\right) \text{ for } h/2 < y \le h \tag{32}$$

$$\tau_w = \frac{\rho_g U_{\text{mean}}^2}{2}\cdot f \tag{33}$$

where f is the fanning friction factor and is computed by,

$$f = 0.0791\cdot \text{Re}^{-0.25}\left(2,800 < \text{Re} < 105^2\right) \tag{34}$$

where Reynolds number Re is defined as,

$$\text{Re} = \frac{U_{\text{free}}h}{\nu} \tag{35}$$

The density ratio of particle to fluid S is 2000 which is consistent with Tian and Ahmadi [19] as well as Zhang and Chen [20] for comparison. In the simulation, the air flow field was calculated to be convergent first, and then the particles were released into the flow field. Particle diameters with 0.1, 0.2, 0.3, 0.5, 1, 2, 3, 5, 10, 20, 30 and 50 μm are studied, as shown in Table 1. For each case, 30,000 spherical particles with uniform distribution were released at $X = 0.2$ because the flow has been fully developed there. The initial particle velocities were equal to the mean velocity of airflow. The gravity force is parallel with the flow direction for vertical duct and perpendicular to the flow direction for horizontal duct.

The governing equations of fluids were solved by the finite volume method. The convection term was discretized by second-order upwind scheme and the diffusion terms were discretized by second-order central difference scheme. The SIMPLE algorithm [41] was adopted to decouple the pressure and velocity fields. The differential equation of particle motion was solved by the Runge-Kutta scheme. The corrections of the wall-normal velocity fluctuations for smooth and ribbed wall cases as well as the velocity and T.K.E distributions in inlet were imposed into FLUENT by UDF codes.

4. Results and discussion

4.1. Air flow simulations and validation

Accurate simulation of turbulent air flow field is the foundation of particle deposition investigation. In order to verify the turbulent air flow filed in this study, the present mean and fluctuating velocities of the air flow in smooth-wall duct were compared with DNS results by Kim et al. [34], as shown in Fig. 3. The mean and fluctuating velocities were obtained at $X = 0.3$ m as the flow has reached full development in this position. It can be observed that the present mean air velocity is in very good agreement with the DNS data shown in Fig. 3(a). Moreover, the streamwise and wall-normal fluctuating velocities obtained by the present RSM model also agree well with the literature results. These agreements indicate that the present turbulent air flow field in smooth-wall duct is

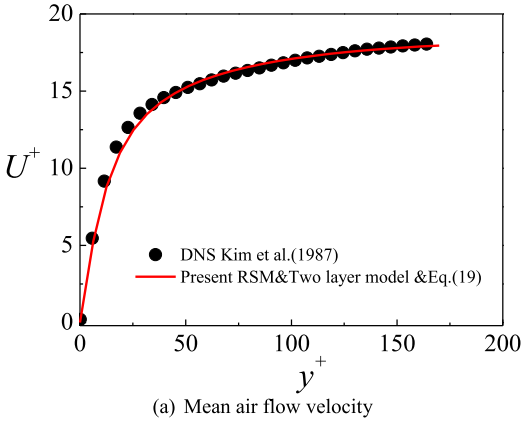

(a) Mean air flow velocity

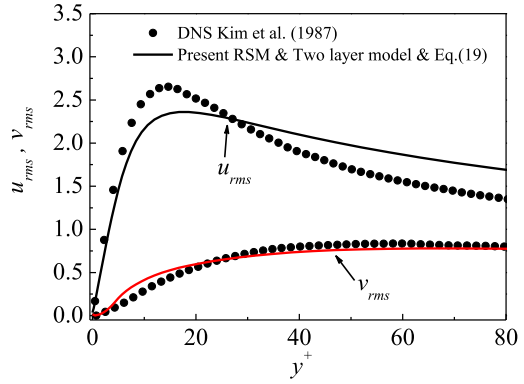

(b) Turbulent fluctuating velocity

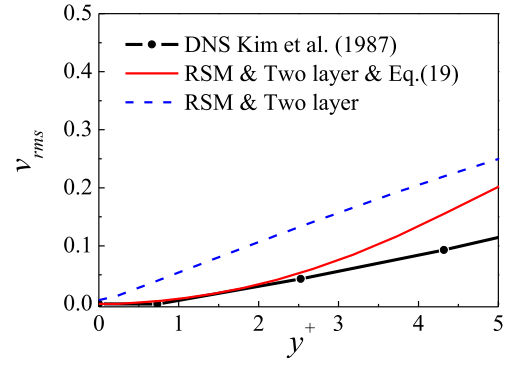

(c) A closer view of wall-normal turbulence fluctuation near wall.

Fig. 3. Comparison of flow velocity profiles for smooth-wall duct with DNS data.

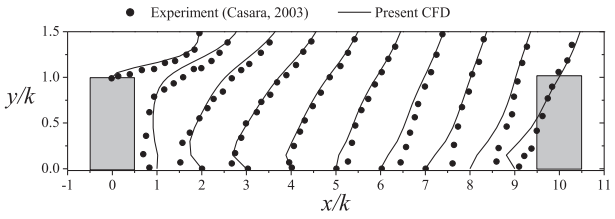

Fig. 4. Air velocity between two adjacent ribs.

valid. Besides, the wall-normal fluctuating velocities near the wall with and without the correction of Eq. (19) were also compared with the DNS data shown in Fig. 3(c). The wall-normal fluctuating velocity with correction agrees much better with DNS results than that without correction. As the wall-normal fluctuating velocity is very important for simulating particle deposition velocity [19,20], it is necessary to modify the turbulent fluctuation in the near-wall region.

Furthermore, the turbulent air flow field in ribbed-wall duct was also verified. It had been found that the flow has reached fully developed state after the 10th rib in ribbed-wall flow [42]. Therefore, the air velocities in different positions between the 11th and 12th ribs were obtained and compared with the experimental results by Casara [38], as shown in Fig. 4. It can be seen that the air flow velocity is consistent with the measurement data in the literature from the figure, implying that the present numerical models and computational grids are able to solve ribbed-duct turbulent flow very well. In consequence, the above validations prove that the present turbulent air flow fields for both smooth- and ribbed-wall flows are credible and correct.

4.2. Particle deposition for smooth wall

Fig. 5 shows the particle deposition velocity in smooth-wall duct air flow, and the results were compared with the previous study data collected by Sippola [43] and other research results [19,20,44].

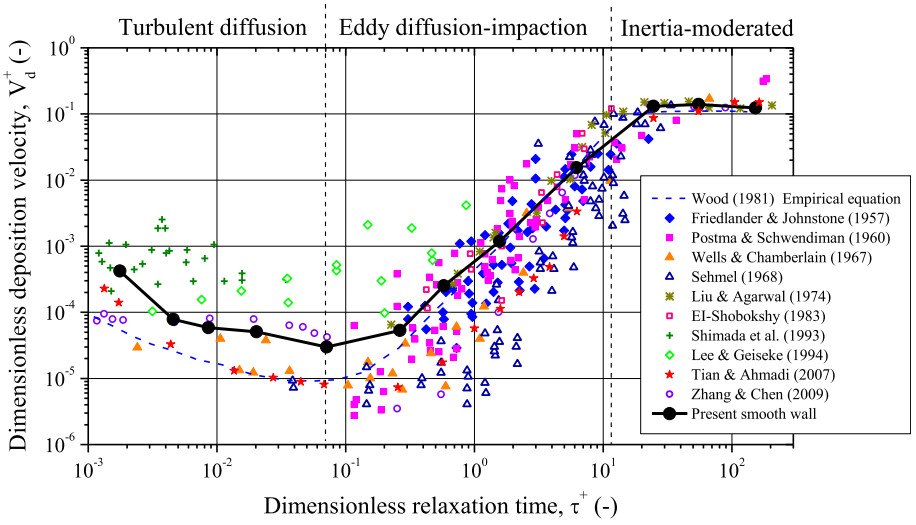

(a) Particle deposition in vertical ducts

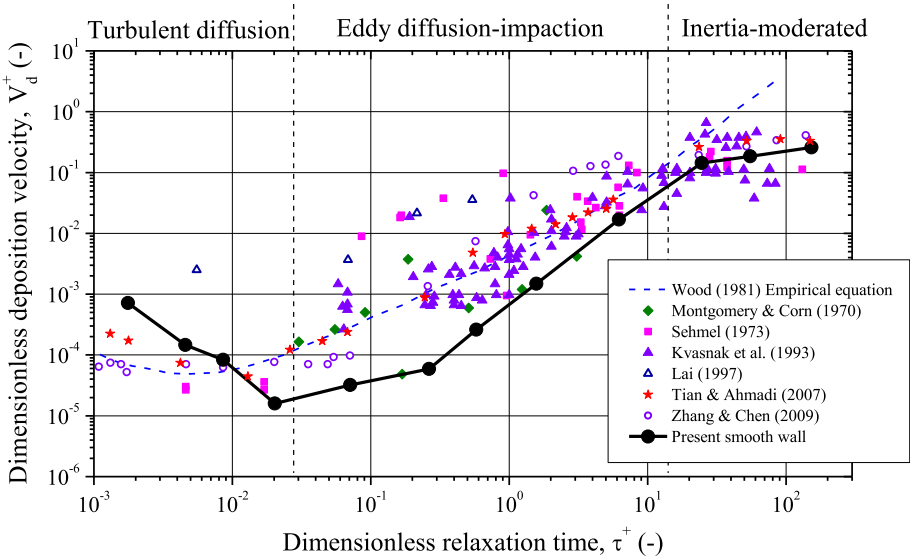

(b) Particle deposition in horizontal ducts

Fig. 5. Particle deposition velocity in air duct flow with smooth wall.

The dimensionless particle deposition velocity was normalized by flow frictional velocity as Eq. (25) while the dimensionless relaxation time of particle was calculated by Eq. (26). Fig. 5(a) and (b) are for vertical and horizontal duct respectively. It is clear that the present particle deposition velocity is in good agreement with the results of Tian and Ahmadi [19] as well as Zhang and Chen [20]. Therefore, it indicates that the RSM model with turbulent fluctuation correction can accurately predict particle deposition velocity as Tian and Ahmadi suggested. According to the researches of Wood [44] and others, particle deposition on smooth surface can be divided into three regions, i.e. turbulent particle diffusion regime, eddy diffusion-impaction regime and inertia-moderated regime. In the turbulent particle diffusion regime, particle deposition is mainly controlled by the combination of Brownian and turbulent eddy diffusions. The particle deposition velocity decreases with the increase of particle relaxation time. In the eddy diffusion-impaction regime, particle deposition is mainly affected by turbulent eddy motion and particle inertia. The particle deposition velocity increases significantly about three to four orders of magnitude. Finally, in the inertia-moderated regime, particle deposition is mainly due to its inertia. The particle deposition velocity keeps constant or decreases slightly with the increase of particle relaxation time. From Fig. 5(a) and (b), it can be seen that the three regimes are clearly distinguished in the present simulation. In fact, Gao et al. [21] pointed out the RSM model can reflect the distinction of the three deposition regimes even without near-wall corrections.

Moreover, the influence of gravity on particle deposition velocity can be found through comparison of Fig. 5(a) and (b). When particle relaxation time is small ($\tau_p^+ < 0.1$), the particle deposition velocity is not affect obviously due to different orientations of gravity. Nevertheless, the particle deposition velocity for horizontal duct case is significantly larger than those for vertical duct case in the inertia-moderated regime ($\tau_p^+ > 10$). It implies that gravity settling becomes increasingly important for coarser particles.

4.3. Enhancement of particle deposition by ribbed wall

To investigate particle deposition enhancement by ribbed surface, dimensionless particle deposition velocities for vertical and horizontal duct cases were obtained shown in Fig. 6. In general, the dimensionless particle deposition velocities are significantly enhanced by ribbed wall in both vertical and horizontal duct cases for the whole sizes of particles. Moreover, it can be observed that the "V" curves of particle deposition are dramatically weakened by ribs, as shown in the figure. This is because the enhancement of particle deposition velocity is significantly discrepant for different particle relaxation times. When $\tau_p^+ < 1$(the turbulent particle diffusion and part of eddy diffusion-impaction regimes), the dimensionless particle deposition velocity can be increased by almost two orders of magnitude by ribbed surface, while it can only be enhanced slightly when $\tau_p^+ > 1$(part of eddy diffusion-impaction and inertia regimes).

In order to observe the particle deposition enhancement more clearly, an enhancement ratio γ was defined as Eq. (36) and given in Fig. 7.

$$\gamma = \frac{v_{d\ \text{rough}}}{v_{d\ \text{smooth}}} \tag{36}$$

The γ is the ratio of dimensional particle deposition velocities between ribbed and smooth duct cases, and the frictional velocity and the associated flow drag are not considered in γ. Therefore, the γ represents the pure enhancement of particle deposition by ribbed surface. A pressure drop-weighted particle deposition enhancement will be discussed in the later section.

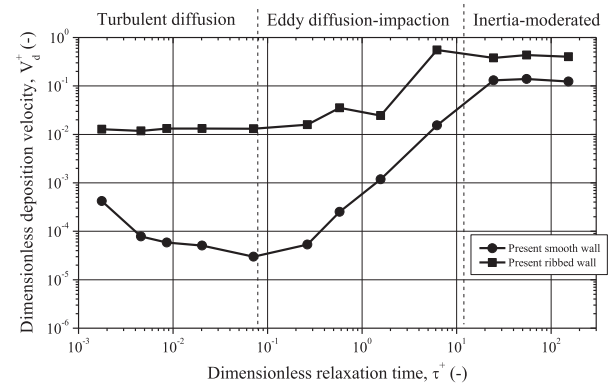

(a) Particle deposition in vertical ducts

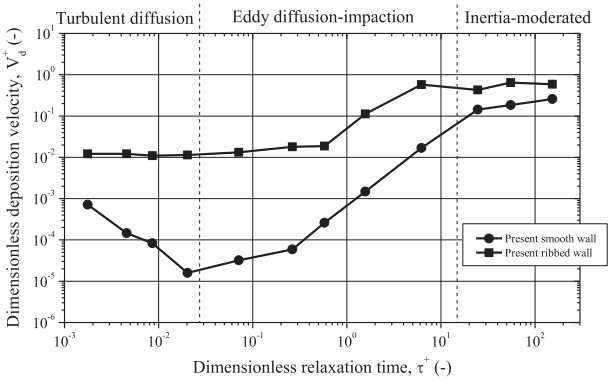

(b) Particle deposition in horizontal ducts

Fig. 6. Enhancement of particle deposition velocity by ribbed wall.

From Fig. 7, it can be found that the enhancement ratio of particle deposition by ribbed surface in vertical duct case is much approximated to that in horizontal one. The agreement between vertical and horizontal duct cases further proves the validation and stability of the present simulations. For horizontal duct case, the maximum enhancement of deposition can reach 4000 times for particle diameter about 0.5 μm, while the minimum enhancement of deposition can reach 13 times for particle diameter about 50 μm. For vertical duct case, the maximum enhancement of deposition can reach 2600 times for particle diameter about 1 μm, while the minimum enhancement of deposition can reach 17 times for particle diameter about 30 μm. Therefore, it can be concluded that the

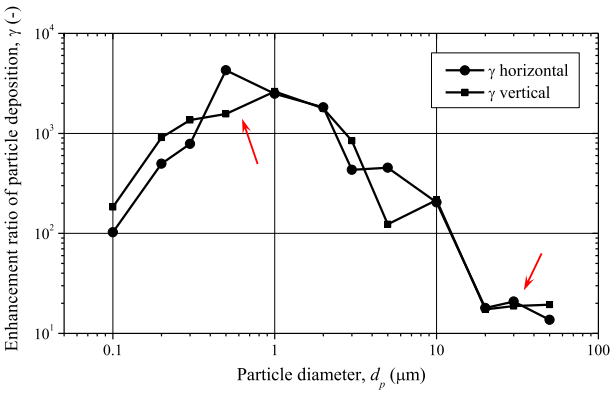

Fig. 7. Enhancement ratio of particle deposition by ribbed wall.

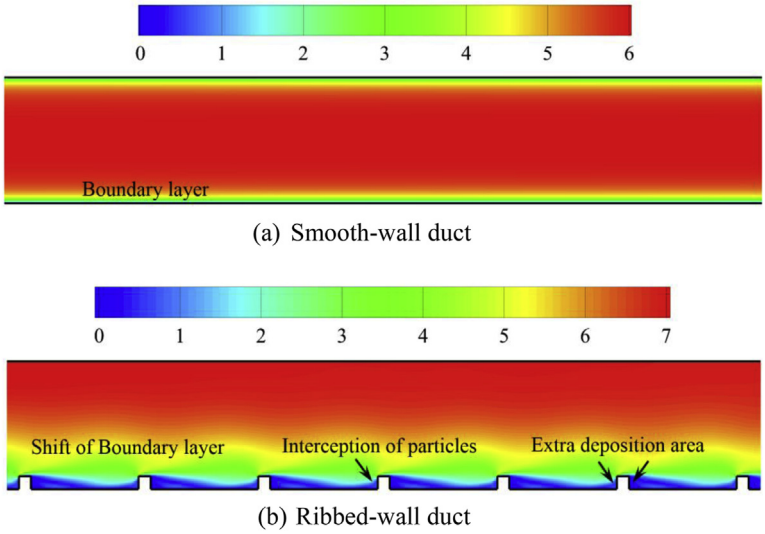

Fig. 8. Velocity contours of air flow in smooth- and ribbed-wall ducts.

particle deposition enhancement is more obvious for small size particles.

4.4. Mechanisms of deposition enhancement by ribs

In this section, the mechanisms of particle deposition enhancement by ribbed surface and the reason why particle deposition velocity increased most for particle size 0.5–1 μm were investigated and discussed. To analyze the issues, Fig. 8 shows the velocity contours of the air flows in smooth- and ribbed-wall ducts, respectively. From the view of physical process, it is obvious that a large number of particles would be obstructed by the windward surface of the ribs along the airflow, as shown by the arrow in Fig. 8(b). This mechanism was also described by Li et al. [7] and Lai et al. [3,4]. Besides, the repeated ribs on the wall increase the particle deposition area dramatically. For smooth wall case, the deposition area is calculated as 0.4 m for two-dimensional duct. For ribbed wall case, it is increased to 0.476 m due to the side surfaces of the ribs shown in Fig. 8(b). The extra deposition area by ribs can reach to 19% compared with the smooth wall case. Furthermore, the high raised surface ribs could decrease the distance of particle settling to the wall. These mechanisms all increase the particle deposition velocity.

Moreover, from the view of turbulent flow structures, the surface ribs have significant influences on the boundary layer flow, including two aspects: the shift of boundary layer and the modification of turbulent structures. Firstly, the boundary layer is shifted by a distance away from the walls because of the surface ribs, i.e. the virtual origin of the velocity profiles is not at the walls, as shown in Fig. 8(b). This effect leads to the reduction of particle deposition distance, which has been also found and investigated by wood [44] for actual wall roughness case.

Secondly, the flow structures of the boundary layer flow are dramatically modified due to the introduction of surface ribs. Fig. 9 illustrates the streamlines of the air flows in smooth- and ribbed-wall ducts, respectively. The results for ribbed wall case are in the cavity between the 11th and 12th ribs. Compared with smooth duct, there are a large-scale separation vortex and a relatively small

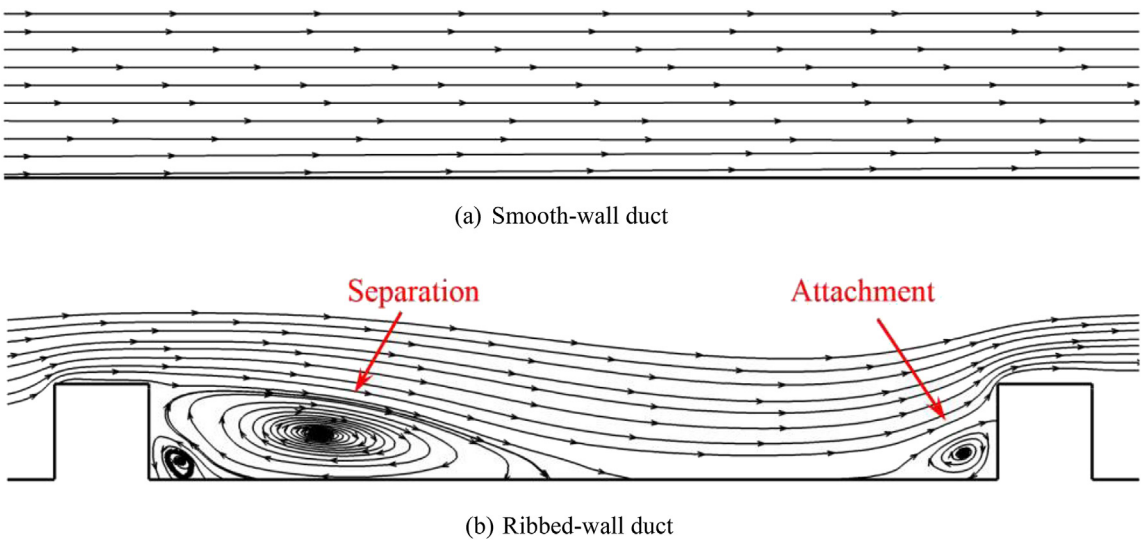

Fig. 9. Streamlines of air flow in smooth- and ribbed-wall ducts.

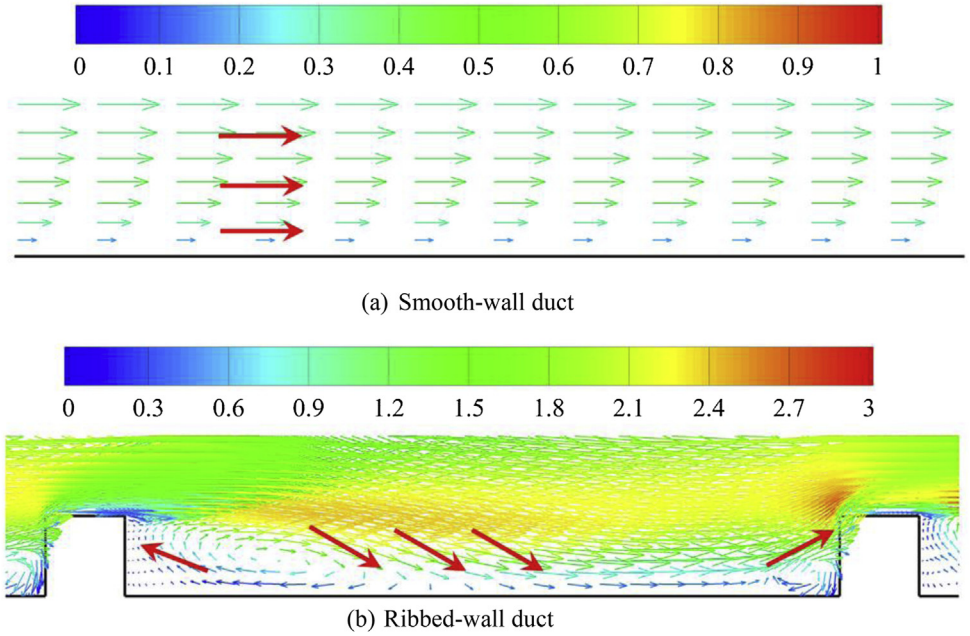

Fig. 10. T.K.E distribution and velocity vectors of air flow in smooth- and ribbed-wall ducts.

attachment vortex induced by surface ribs in each repeated rib cavity displayed in Fig. 9(b). These vortex structures for ribbed-duct lead to much more complex boundary layer than those for smooth duct.

Fig. 10 shows distributions of turbulent kinetic energy (T.K.E.) of the air flows in smooth- and ribbed-wall ducts, respectively. The results for ribbed wall case are also in the cavity between the 11th and 12th ribs. The colors and arrows represent the magnitude of T.K.E. and velocity vectors of fluids, respectively. It can be observed that the near-wall T.K.E. distribution for smooth duct is from zero to about 1 J/kg. The T.K.E. of airflow is low and the velocity vectors are along the flow direction. However, the intense T.K.E. is produced by turbulent eddies to the wall and windward surfaces of the ribs, as shown in Fig. 10(b). The maximum T.K.E. near the wall increases to 3 J/kg, which is much higher than those for smooth duct case. Moreover, the airflow velocity vectors with high T.K.E are towards the wall and side surfaces of the ribs, as shown by the arrows in Fig. 10(b). Therefore, once particles move into the turbulent eddy regions, they would probably be captured and entrained to the wall or the windward surfaces of ribs by the eddies. These modifications of turbulent structures and the T.K.E. distribution in boundary layer by surface ribs are beneficial to enhance particle deposition. Furthermore, this mechanism would enhance much more particle deposition for the particles of small relaxation time ($\tau_p^+ < 1$), because small particles are easy to be controlled by turbulent eddy diffusion. However, the capture capacity of these turbulent eddies is insufficient for particles with large relaxation time ($\tau_p^+ > 1$) due to the large inertia of these particles. Therefore, the maximum enhancement of particle deposition occurs for particle diameter about 0.5–1 μm due to the influence of turbulent eddies.

4.5. Efficiency ratio of particle deposition

Finally, an efficiency ratio of particle deposition was defined and discussed to evaluate the particle deposition enhancement considering the increase of pressure drop. The gain of ribbed surface is particle deposition increase while the loss is more flow drag.

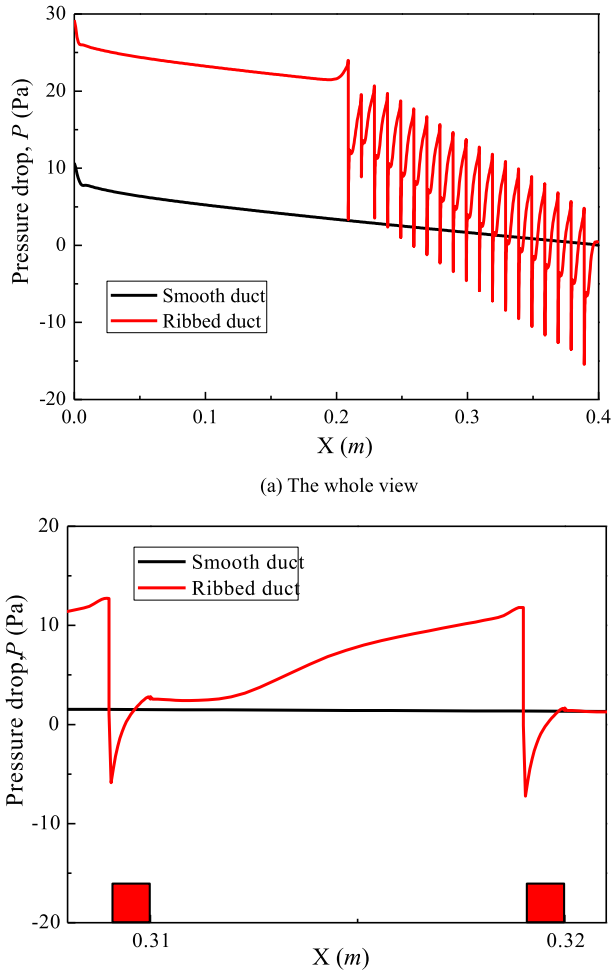

Fig. 11. Pressure drop of air flow in smooth- and ribbed-wall ducts.

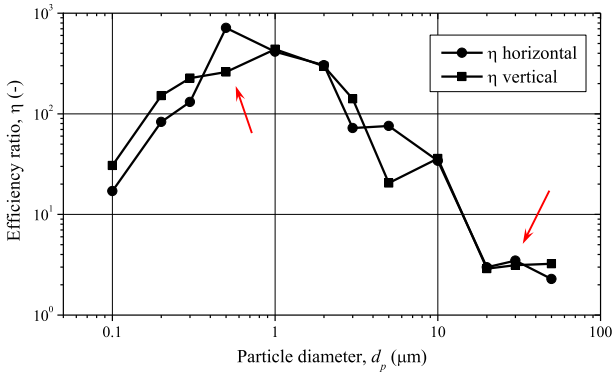

Fig. 12. Efficiency ratio of particle deposition by ribbed wall.

Therefore, a pressure drop-weighted particle deposition enhancement was defined as follows,

$$\eta = \frac{v_{d\ \mathrm{rough}}}{v_{d\ \mathrm{smooth}}} \cdot \frac{f_{\mathrm{smooth}}}{f_{\mathrm{rough}}} \tag{37}$$

where the $f_{\mathrm{rough}}/f_{\mathrm{smooth}}$ is the increase of flow drag.

To investigate the increase of flow drag by surface ribs, Fig. 11 shows the pressure drop for smooth- and ribbed-wall duct. Fig. 11(a) and (b) are the whole view for the ducts and the enlarged view for the cavity between the 11th and 12th ribs, respectively. From Fig. 11(a), it can be observed that the pressure distribution curve is stably decreased for smooth wall case. The value of the pressure at $X = 0.2$ m is about 3.5 Pa which is the released position of particles. Nevertheless, the pressure profile presents intense oscillation with periodic peaks and nadirs after $X = 0.2$ m due to the disturbance of repeated surface ribs. From Fig. 11(b), it is clearer that a peak value of pressure occurs at the windward surface of the ribs because of the form drag. Then, it rapidly drops into a nadirs on the crest of ribs and increases relatively slowly but nonlinearly to the next peak. The negative pressure appears due to the backflow in the cavity. It is found that the pressure value is about 21 Pa at $X = 0.2$ m for ribbed wall duct. The ratio of pressure drop for the two cases is about 6. Therefore, the ratio of flow drag between ribbed and smooth wall cases$f_{\mathrm{rough}}/f_{\mathrm{smooth}} \approx 6$ in the study.

The efficiency ratio η versus particle diameter is demonstrated in Fig. 12. It can be found that the maximum efficiency ratio for vertical and horizontal duct cases can reach more than 100 for particle diameter about 0.2–3 μm, while the minimum efficiency ratio can reach about 3 for particle diameter about 20–50 μm. Therefore, the ribbed surface could be effective and efficient for particle deposition enhancement of PM 2.5 (fine particles less than 2.5 μm).

5. Discussion

In this study, the efficiency ratio can reach more than 100 for particles of 0.2–3 μm. However, the similar efficiency ratio was calculated to be 1.77 to 1.89 for particle sizes 0.7–7.1 μm in the experimental study by Lai et al. [3,4]. The main reason of this huge deviation is that the particle deposition enhancement is measured only for the 11th to 14th ribs in their study while it is calculated for the whole 19 ribs here, except other minor differences such as duct and rib sizes as well as the number of ribs. It is obvious that a large number of particles would be obstructed by the first several ribs. Therefore, the simulation results cannot be compared with the experiment data of Lai et al. Besides, it has been confirmed that the particle deposition velocity would be increased by surface roughness for two orders of magnitudes in the particle diffusion regime, even at very small values (Liu and Agarwal 1974; Li and Ahmadi 1993; Guha 1997, 2008; Hussein et al., 2012) [45–47,35,9]. The surface roughness also has significant influence on particle deposition velocity in the diffusion-impaction regime [43–45,35,9]. Therefore, the efficiency ratio obtained in this simulation is reasonable.

6. Conclusions and future work

This paper investigated the particle deposition in turbulent duct air flow with both smooth and ribbed walls. The enhancement and mechanism of particle deposition by surface ribs were analyzed and discussed, and the following conclusions can be obtained,

1. The particle deposition velocity is significantly increased for almost 10–4000 times by the ribbed wall both for the vertical and horizontal duct cases. The maximum enhancement of particle deposition occurs for 0.2–3 μm particles while the minimum enhancement appears for 20–50 μm particles.
2. The enhancement of particle deposition is because of the obstruction of ribs, increase of deposition area and decrease of deposition distance to the wall. Moreover, for the particles in the turbulent diffusion and eddy diffusion-impaction regimes, the particle deposition is extremely enhanced due to the captures of the turbulent eddies and large T.K.E to the wall. For particles in the inertia-moderated regime, the influence of turbulent eddy on particle deposition is relatively slight due to particle inertia.
3. For the present $p_r/k_r = 10$ ribbed wall, the pressure drop-weighted efficiency ratio of particle deposition enhancement can reach more than 100 for 0.2–3 μm particles compared with that of smooth wall case. It can also be 3 for particle sizes 20–50 μm. Therefore, arrangement of repeated ribs on the duct wall could be a highly efficient way for particle deposition enhancement and particle capture, especially for micron particles such as PM2.5.

In addition, the influences of different rib height k_r and different spacing to height ratio p_r/k_r on the particle deposition enhancement by ribbed-surface need to be further investigated. Moreover, the accumulation of particles would also be resuspended in the ventilation ducts [48], which may weaken the deposition rate of the particles. This effect should be carefully investigated in further work.

Acknowledgment

The authors appreciate the financial supports provided by Central Policy Unit of the Hong Kong Government via the Public Policy Research Scheme (2013.A6.010.13A).

References

[1] Vincent JH, MacLennan ASM. Aerodynamic considerations in electrostatic precipitator. J Electrost 1980;8:325–42.
[2] Suh YJ, Kim SS. Effect of obstructions on the particle collection efficiency in a two-stage electrostatic precipitator. J Aerosol Sci 1996;27:61–74.
[3] Lai ACK, Byrne MA, Goddard AJH. Measured deposition of aerosol particles on a two-dimensional ribbed surface in a turbulent duct flow. J Aerosol Sci 1999;30:1201–14.
[4] Lai ACK, Byrne MA, Goddard AJH. Enhanced particle loss in ventilation duct with ribbed surface. Build Environ 2000;35:425–32.
[5] Sun K, Lu L. Particle flow behavior of distribution and deposition throughout 90° bends: analysis of influencing factors. J Aerosol Sci 2013;65:26–41.
[6] Sun K, Lu L, Jiang H, Jin HH. Experimental study of solid particle deposition in 90° ventilated bends of rectangular cross section with turbulent flow. Aerosol Sci Technol;47:115–124.

[7] Li A, Ahmadi G, Bayer RG, Gaynes MA. Aerosol particle deposition in an obstructed turbulent duct flow. J Aerosol Sci 1994;25:91–112.
[8] Iacono GI, Tucker P, Reynolds A. Predictions for particle deposition from LES of ribbed channel flow. Int J Heat Fluid Flow 2005;26:558–68.
[9] Hussein T, Smolik J, Kerminen V, Kulmala M. Modeling dry deposition of aerosol particles onto rough surfaces. Aerosol Sci Technol 2012;46:44–59.
[10] Lai ACK, Nazaroff WW. Modelling indoor particle deposition from turbulent flow onto smooth surfaces. J Aerosol Sci 2000;31:463–76.
[11] Zhao B, Wu J. Modeling particle deposition from fully developed turbulent flow in ventilation duct. Atmos Environ 2006;40:457–66.
[12] Zhao B, Wu J. Modeling particle deposition onto rough walls in ventilation duct. Atmos Environ 2006;40:6918–27.
[13] Piskunov VN. Parameterization of aerosol dry deposition velocities onto smooth and rough surfaces. J Aerosol Sci 2009;40:664–79.
[14] Barth T, Reiche M, Banowski M, Oppermann M, Hampel U. Experimental investigation of multilayer particle deposition and resuspension between periodic steps in turbulent flows. J Aerosol Sci 2013;64:111–24.
[15] Lecrivain G, Drapeau-Martin S, Barth T, Hampel U. Numerical simulation of multilayer deposition in an obstructed channel flow. Adv Powder Technol 2014;25:310–20.
[16] Chen Q. Ventilation performance prediction for buildings: a method overview and recent applications. Build Environ 2009;44(4):848–58.
[17] Zhang Z, Chen Q. Comparison of the Eulerian and Lagrangian methods for predicting particle transport in enclosed spaces. Atmos Environ 2007;41:5236–48.
[18] Gao NP, Niu JL. Modeling particle dispersion and deposition in indoor environments. Atmos Environ 2007;41:3862–76.
[19] Tian L, Ahmadi G. Particle deposition in turbulent duct flows-comparisons of different model predictions. J Aerosol Sci 2007;38:377–97.
[20] Zhang Z, Chen Q. Prediction of particle deposition onto indoor surfaces by CFD with a modified Lagrangian method. Atmos Environ 2009;43:319–28.
[21] Gao N, Niu J, He Q, Zhu T, Wu J. Using RANS turbulence models and Lagrangian approach to predict particle deposition in turbulent channel flows. Build Environ 2012;48:206–14.
[22] Jiang H, Lu L, Sun K. Simulation of particle deposition in ventilation duct with a particle-wall impact model. Build Environ 2010;45(5):1184–91.
[23] Jiang H, Lu L, Sun K. Experimental study and numerical investigation of particle penetration and deposition in 90 degrees bent ventilation ducts. Build Environ 2011;46:2195–202.
[24] Jiang H, Lu L, Sun K. Computational fluid dynamics (CFD) modelling of particle deposition in a two-dimensional turbulent channel air flow: study of influence factors. Indoor Built Environ 2012;21(2):264–72.
[25] Sun K, Lu L, Jiang H. Modelling of particle deposition and rebound behaviour on ventilation ducting wall using an improved wall model. Indoor Built Environ 2011;20(3):300–12.
[26] Sun K, Lu L, Jiang H. A computational investigation of particle distribution and deposition in a 90° bend incorporating a particle-wall model. Build Environ 2011;46:1251–62.
[27] Sun K, Lu L, Jiang H. A numerical study of bend-induced particle deposition in and behind duct bends. Build Environ 2012;52:77–87.
[28] Launder BE, Reece GJ, Rodi W. Progress in the development of a Reynolds stress turbulent closure. J Fluid Mech 1975;68(3):537–66.
[29] Wolfstein M. The velocity and temperature distribution of one-dimensional flow with turbulence augmentation and pressure gradient. Int J Heat Mass Transf 1969;12(3):301–18.
[30] Chen HC, Patel VC. Near-wall turbulence models for complex flows including separation. AIAA J 1988;26:641–8.
[31] Jongen T. Simulation and modeling of turbulent incompressible flows [PhD thesis]. Lausanne, Switzerland: EPF Lausanne; 1992.
[32] Fluent Inc. FLUENT 12.0 user's guide. Lebanon, NH. 2009.
[33] Ounis H, Ahmadi G. Analysis of dispersion of small spherical particles in a random velocity field. J Fluids Eng 1990;112:114–20.
[34] Kim J, Moin P, Moser R. Turbulence statistics in fully developed channel flow at low Reynolds number. J Fluid Mech 1987;177:133–66.
[35] Guha A. Transport and deposition of particles in turbulent and laminar flow. Annu Rev Fluid Mech 2008;40:311–41.
[36] Liou TM, Hwang JJ, Chen SH. Simulation and measurement of enhanced turbulent heat transfer in a channel with periodic ribs on one principal wall. Int J Heat Mass Transf 1993;36:507–17.
[37] Okamoto S, Seo S, Nakaso K, Kawai I. Turbulent shear flow and heat transfer over the repeated two-dimensional square ribs on ground plane. ASME Trans J Fluid Eng 1993;115:631–7.
[38] Casarsa L. Aerodynamic performance investigation of a fixed rib-roughened internal cooling passage [PhD. thesis]. Belgium: Von Karman Institute for Fluid Dynamics; 2003.
[39] Schlichting H. Boundary-layer theory. New York: McGraw Hill; 1979.
[40] Schlichting H, Gersten K. Boundary-layer theory. 8th ed. Berlin: Springer; 2000.
[41] Partankar SV. Numerical heat transfer and fluid flow. Washington, DC: Hemisphere; 1980.
[42] Liou TM, Wang WB, Chang YJ. Holographic interferometry study of spatially periodic heat transfer in a channel with ribs detached from one wall. ASME Trans J Heat Transf 1995;117:32–9.
[43] Sippola MR. Particle deposition in ventilation ducts [PhD. dissertation]. Berkeley, CA, USA: University of California; 2002.
[44] Wood NB. A simple method for the calculation of turbulent deposition to smooth and rough surfaces. J Aerosol Sci 1981;12:275–90.
[45] Liu BYH, Agarwal JK. Experimental observation of aerosol deposition in turbulent flow. J Aerosol Sci 1974;5:145–55.
[46] Li A, Ahmadi G. Computer simulation of deposition of aerosols in a turbulent channel flow with rough walls. Aerosol Sci Technol 1993;18:11–24.
[47] Guha AA. Unified Eulerian theory of turbulent deposition to smooth and rough surface. J Aerosol Sci 1997;28:1517–37.
[48] Zhou B, Zhao B, Tan ZC. How particle resuspension from inner surfaces of ventilation ducts affects indoor air quality-a modeling analysis. Aerosol Sci Technol 2011;45:996–1009.

Glossary

C_0: mean particle concentration
F_S: Saffman's lift force
f: fanning friction factor
f_{rough}: flow drag for rough duct
f_{smooth}: flow drag for smooth duct
h: duct height
J: number of particles deposited per unit time and unit area
k: turbulent kinetic energy (T.K.E.)
k_r: rib height
$\overline{p}$: time-averaged pressure
p_r: rib spacing
Re: Reynolds number
S: ratio of particle-to-fluid density
T_L: fluid Lagrangian integral time scale
U_{mean}: mean velocity of air
U_{free}: freestream velocity of air
u_g: velocity of fluid
$\overline{u}_i$: time-averaged velocity
u_p: velocity of particle
u'_{rms}: streamwise fluctuating velocity of air
V_d: particle deposition velocity
V_d^+: dimensionless particle deposition velocity
$v_{d\,rough}$: particle deposition velocity on ribbed-duct
$v_{d\,smooth}$: particle deposition velocity on smooth duct
v'_{rms}: wall-normal fluctuating velocity of air
w'_{rms}: spanwise fluctuating velocity of air
u^*: frictional velocity of air
y^+: dimensionless distance from the wall

Greek symbols

ε: dissipation rate of turbulent kinetic energy
ρ_g: density of fluid
ρ_p: density of particle
ζ: normal distributed random number
μ: dynamic viscosity of air
ν: kinetic viscosity of air
γ: ratio of dimensional particle deposition velocities between ribbed and smooth duct cases
η: a pressure drop-weighted particle deposition enhancement
τ_p^+: dimensionless particle relaxation time